PROCEEDINGS, 42nd Workshop on Geothermal Reservoir Engineering
Stanford University, Stanford, California, February 13-15, 2017
SGP-TR-212

Assessment of the Geothermal Potential of the Gediz Graben, Manisa, Turkey

Selim Cambazoğlu[1], Arif Mert Eker[2], Gözde Yal[1], Osman Şen[2], Hüseyin Dünya[3], Haluk Akgün[1]

[1] Geotechnology Unit, Department of Geological Engineering, Middle East Technical University, Ankara, Turkey

[2] SDS Energy, Ankara, Turkey

[3] General Directorate of Mineral Research and Exploration, Aegean Regional Directorate, İzmir

selimcambaz@gmail.com

Keywords: GIS, Bivariate correlation, Gediz Graben, Turkey

ABSTRACT

The study covers quantitative correlation and comparison of geothermal gradient data with various explanatory variables for the Gediz Graben, Manisa Province. Although Turkey has a high geothermal potential and is among the top ten countries producing power through geothermal energy, the main resource for power generation still remains to be fossil fuels. Only 1% of the total power generation of Turkey is from geothermal energy. However, the advantageous geological conditions in Turkey along with the technological developments as well as the regulations issued on geothermal energy in the last decade have allowed geothermal energy to be economically favorable. In light of these technological and legislative developments, geothermal exploration in Turkey has accelerated in the recent years especially in Büyük Menderes Graben and Gediz Graben. In Turkey, Gediz Graben currently ranks as second in geothermal energy production having 118 MWe power generation capacity with high potential for further development. Therefore, this study includes the spatial and statistical assessment of the available geothermal well data with geological, seismo-tectonic, topographic, surface temperature and vegetation data within a GIS environment for the Gediz Graben, Manisa Province. Bottom hole temperature and depth data from more than 90 geothermal wells were used to generate a geothermal gradient map. The explanatory datasets were statistically evaluated and their relationship with geothermal gradient has been assessed.

1. INTRODUCTION

Currently, Turkey is one of the most promising countries in terms of geothermal development. Turkey ranks 7th in the world in terms of installed capacity with a total capacity of 821 MWe with 31 active geothermal power plants. The majority of these power plants are located within the Büyük Menderes Graben (689 MWe in Aydın and Denizli Provinces) and Gediz Graben (Manisa Province) hosting a total of 4 geothermal power plants having 118 MWe installed capacity. Further, geothermal power plants currently under construction and at planning stage for Manisa Province have approximately 50 MWe capacity.

In this study, geothermal gradient data is correlated with various geological, morphological, seismo-tectonic, vegetation and surface temperature data. In order to assess the geothermal potential, datasets such as topographical maps, active fault map, Bouger gravity anomaly, earthquake epicenter catalogue, Landsat and ASTER satellite image data were used. These datasets were further assessed to generate maps of explanatory variables. The geothermal gradient map was used as the dependent variable while the explanatory variables including Digital Elevation Model (DEM), slope, Normalized Difference Vegetation Index (NDVI), Gutenberg-Richter b-value, fault density, distance to graben center and ASTER night-time surface temperature data were used as the independent variables. The geothermal gradient map was generated through interpolation of borehole data from General Directorate of Mineral Research and Exploration (MTA) and various private companies. Each variable layer was incorporated into a GIS environment and a bivariate correlation analysis between the dependent variable and explanatory variables were performed.

2. STUDY AREA AND GENERAL GEOLOGY

Manisa Province is located in the Western Anatolia, Turkey and covers approximately 13250 km2 area in a region delineated by various horst and graben systems. Western Anatolia is one of the most important regions in the world in terms of geothermal energy potential, with considerable seismic activity and rapid extension in N-S direction at a rate of 30-40 mm/year (Bozkurt, 2001).

The study area is situated on the E-W and WNW-ESE trending Gediz Graben at the southern section of the Manisa Province. The Gediz Graben is bounded by the Bozdağ Mountains in the south and by various ENE-WSW trending horst and graben systems in the north. These graben systems (from east to west: Gördes Graben, Dilekdağ-Demircidağ Horst, Demirci Graben, Icikler Horst, Selendi Graben, Umurbaba-Rahmanlar Horst and Güre Graben) reaches the E-W trending Simav Graben at the north of the region which lies parallel to the eastern part of the northern boundary of the Manisa Province (Yılmaz et al., 2000; Klingel et al., 2015) (Figure 1).

The Gediz Graben have an approximate E-W and WNW-ESE trend with 140-150 km length and 10-40 km width (Yılmaz et al., 2000; Bozkurt and Sözbilir, 2004). The extent of this study covers around 100 km lenght of the Gediz Graben starting from the western end to the south of Alaşehir district at the southeast, encompassing around 2800 km2 area and Turgutlu, Ahmetli, Salihli and Alaşehir districts. The faults bounding the northern margin of the Gediz Graben are morphologically less marked and seismically inactive. Different from the northern margin, the southern margin of the Gediz Graben is steeper and seismically more active and bounded by a major fault zone

consisting of a number of steep (>70°) north dipping normal faults along with a low angle detachment fault (~10°). South of the graben margin, lies the steep Bozdag Mountain (Horst) (Yılmaz et al., 2000; Çiftçi and Bozkurt, 2009) which causes a sharp elevation change.

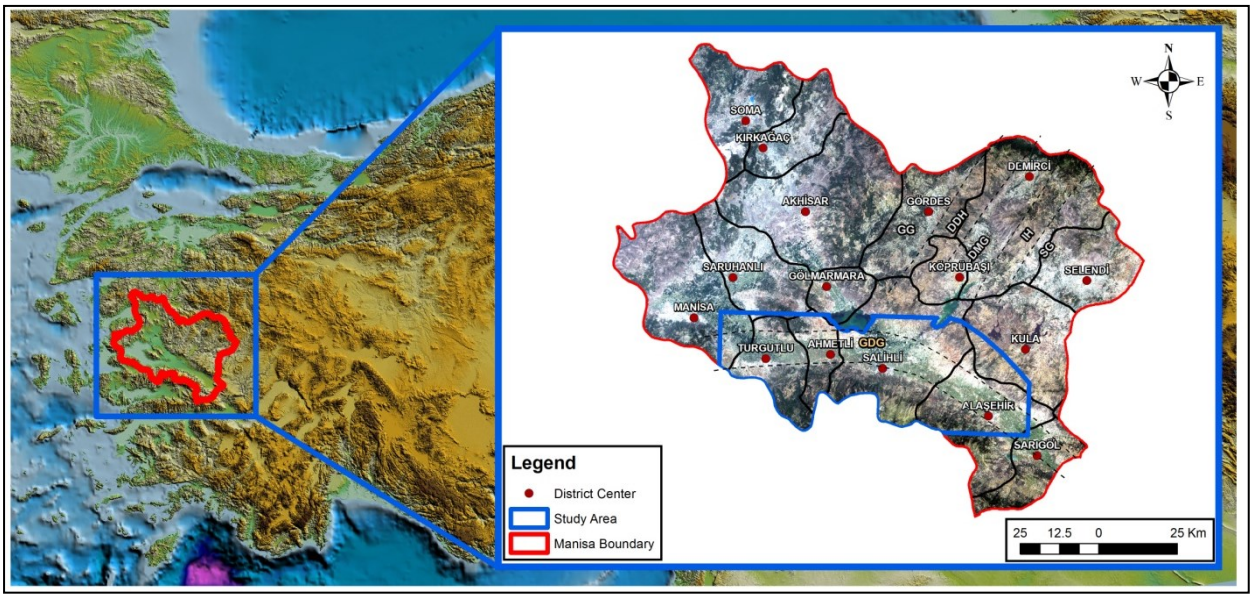

Figure 1: Location map showing extent of the confined study area in blue color boundary over true color Landsat image (GDG: Gediz Graben, GG: Gördes Graben, DDH: Dilekdağ-Demircidağ Horst, DG: Demirci Graben, IH: Icikler Horst, SG: Selendi Graben).

The basement rock unit at the study area is the Paleozoic-Mesozoic Menderes Metamorphics. This unit is composed of granitic augen-gneiss, various gneisses, metavolcanics and metasedimentary units. The metasedimentary units of Paleozoic-Early Tertiary age are moderate to low degree metamorphosed schist, quartz-schist, calc-schist and marbles. The basement Menderes Massif is unconformably overlain by Neogene Alaşehir Group and which is further overlain by the Kızıldağ Groups (Yılmaz et al., 2000). The Miocene-Pliocene sequence is overlain by Plio-Quaternary and Quaternary alluvial deposits. The Miocene rock units are continental clastics and carbonates which serve as the cap rock of the geothermal system in the region whereas the Paleozoic-Mesozoic Menderes Metamorphics serve as the reservoir rocks of the geothermal system (Yılmazer et al., 2010).

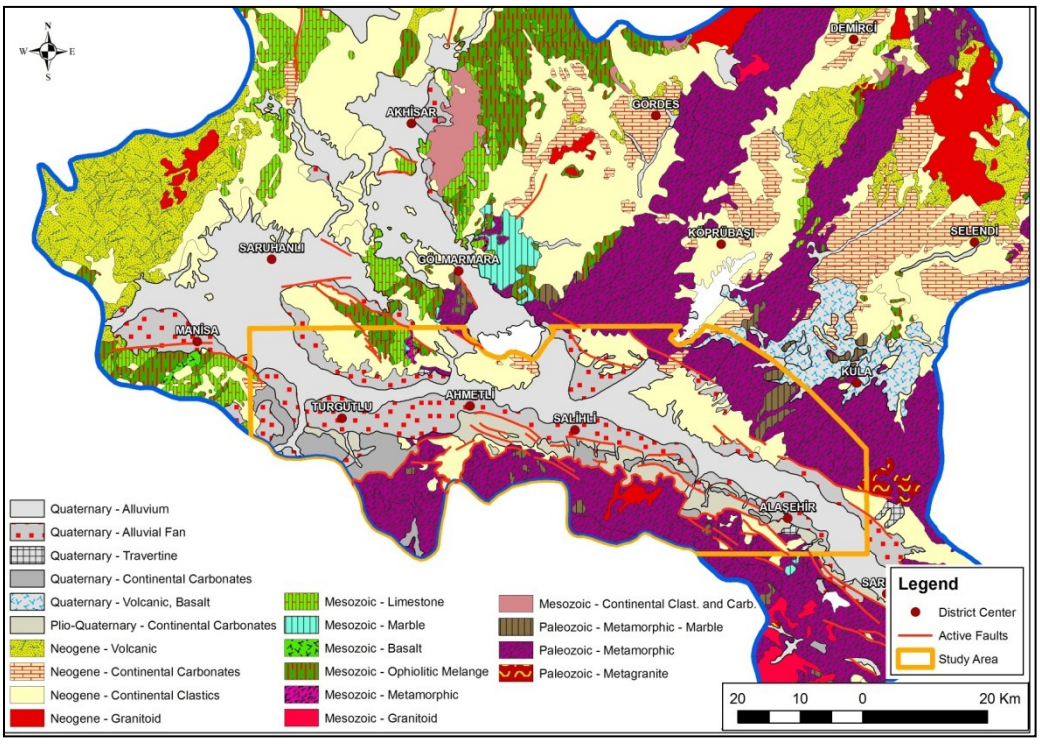

Figure 2: Generalized geological map of the study area and its surroundings (Adapted from: MTA, 2002).

3. DATA SETS AND METHODOLOGY

The development of a geothermal system depends on the existence of four major factors i) a natural heat source such as cooling magma, ii) sufficient fluid flow, iii) aquifer or a permeable reservoir and iv) an impervious cover rock (Ozgüler et al., 1983). Heat source of a hydrothermal system can be young dykes and plutons (Elders et al., 1984; Henley and Brown, 1985; Wohletz and Heiken, 1992; Embley et al., 1995), increase in subsurface temperatures as a result of tectonic activity (McKendiz, 1978; Henley and Brown, 1985) and frictional heat due to fault activity (Lachenbruch, 1980; Scholz, 1980). Highly permeable media that allows thermal fluid upwell can be either unconfined aquifers, layer planes (Person et al., 1996), volcanic contact zones (e.g. sill, dyke) (Martel and Petersen, 1991; Boullier et al., 1994), or can be closely correlated with structural features (Curewitz and Karson, 1997, Micklethwaite and Cox, 2004, Faulds et al., 2011) when regional studies are considered. The structural features along with the data to be acquired from studies incorporating geological factors (Prol-Ledesma, 2000; Yousefi et al., 2007; Noorollahi et al., 2008); solar radiation (Voulgaris et al., 2004), hydrothermal alteration types (Browne, 1977; Henley and Ellis, 1985; Yousefi et al., 2007; Noorollahi et al., 2008; Marques et al., 2010), magnetic anomaly (Tüfekçi et al., 2010), gradient temperature (Voulgaris et al., 2004), identification of thermal water outlet points (Prol-Ledesma, 2000; Coolbaugh and Shevenell, 2004; Yousefi et al., 2007; Carranza et al., 2008), identification of potential reservoir rocks (Prol-Ledesma, 2000; Carranza et al., 2008; Tüfekçi et al., 2010),and identification of surface temperature anomalies (Coolbaugh et al., 2002; MacKnight et al., 2004; Voulgaris et al., 2004; Calvin et al., 2005; Eneva et al., 2006, 2007; Coolbaugh et al., 2007a; Gutierrez et al., 2012; Haselwimer and Prakash, 2013) can be of great importance for the assessment of a geothermal field.

In scope of this study, geothermal gradient data, DEM, slope, NDVI, b-value, fault density, distance to graben and ASTER night-time surface temperature layers were introduced into a GIS environment and their spatial distributions were correlated (Figure 3). Source and scale/resolution information of these datasets are presented in Table 1. As can be seen from the table, the datasets have different scale and spatial resolution, therefore, in order to compile a spatially consistent database, all datasets were resampled to 90 m x 90 m pixel resolution consistent with the resolution of the ASTER thermal infrared images. Although most of the explanatory variables were prepared in order to cover the Manisa provincial area, the extent of the area of interest was further confined according to the interpolated geothermal gradient map generated from the well data. This confined area corresponds roughly to the extent of the Gediz Graben at the southern section of the Manisa province. The descriptive statistics of the datasets are presented in Table 1 for the study area.

Digital Elevation Model (DEM) layer was prepared by digitizing the contour lines of the 1:25.000 scale topographical maps of General Command of Mapping (HGK) (Figure 3a). The elevation values range between 5 m and 2120 m for the entire area. The slope layer was generated by using DEM data via ArcGIS 9.3 software and the regional slope values ranged between 0º and 57º (Figure 3b). On the other hand, the elevation and the slope values ranged between 5 m and 2056 m, and 0º and 41º respectively for the area of interest.

For the generalized geological map, 1:500.000 scale geological map prepared by the General Directorate of Mineral Research and Exploration (MTA, 2002) was used. The map was digitized and classified according to age and lithology type as a vector layer (Figure 2). It was observed that most of the well data is located within the Quaternary alluvium graben basin area.

For the NDVI layer, Visible Red (RED) and Near Infrared (NIR) bands of Path: 180, Row: 33 Landsat 8 OLI&TIRS image acquired on June 20, 2016 (USGS-EROS, 2017) and having 30 m x 30 m resolution was used. The NDVI layer was formed by using (NIR-RED)/(NIR-RED) relation, which represents the density of green bio-mass and ranges between -1 and +1. Higher NDVI values indicate healthy and densely vegetated areas (Figure 3c).

Another sattlite dataset, night-time surface temperature, is generated from 5 different ASTER L1T image data (NASA LP DAAC, 2015), courtesy of the NASA Land Processes Distributed Active Archive Center (LP DAAC), USGS/Earth Resources Observation and Science (EROS) Center, Sioux Falls, South Dakota. The spatial resolution of the ASTER Thermal Infrared (TIR) bands is 90 m x 90 m while the spectral range of the five TIR bands is between 8.125 and 11.65 μm. A total of 5 ASTER images where two image pairs located at the eastern part (acquisition date: February 7, 2011), two image pairs located at the western part (acquisition date: December 5, 2016) and a single image (acquisition date: November 23, 2003) joining these two pairs were used. Surface temperature was obtained from TIR data for each image separately by utilizing emissivity and temperature separation algorithm (Hook et al., 1992; Gillespie et al., 1998). In order to create an almost seamless mosaic image, the eastern pair was taken as reference and surface temperature of the central image was scaled according to the mean and standard deviation of the overlapping region between this single image and the eastern pair. The same process was repeated for the central image and the western pair, and the surface temperature values of the western pair was re-calculated accordingly. Elevation correction was performed on the mosaic image by considering an environmental lapse rate of -6.5ºC/km which is considered to be suitable for most cases (Eneva and Coolbaugh, 2009, Gutierrez et al., 2012). Thus, the elevation corrected mosaic of these five images were used as the explanatory variable (Figure 3d).

In order to represent the seismo-tectonic framework of the study area, fault density and Gutenberg-Richter b-value maps were prepared. The fault density map was prepared by initially digitizing fault data from various studies in the literature (MTA, 2002; Yılmazer et al., 2010; Duman et al., 2011; Klingel et al., 2015) thus compiling a generalized line source map. The fault density map was generated by using this line source layer and 5.2 km search radius. This radius was identified by considering the average earthquake epicenter depth falling within the study area (9 km) (KOERİ, 2016) and fault dip angle of 60º (Shah, 2015). The faults within the region are mostly either high angle dipping normal faults with minor strike slip component or low angle detachment faults (Shah, 2015). According to focal mechanism solutions of the earthquakes within the study area, the dip angle of the faults generating these earthquakes ranges between 28º and 89º with an average value of 60º. Therefore, by using this epicenter depth of 9 km and fault dip angle of 60º a search radius of 5.2 km was determined. The fault density map was prepared with a resolution of 90 m x 90 m as well (Figure 3e).

The second seismo-tectonic parameter, the Gutenberg-Richter (1949) b-value map was generated by using Z-Map (Weimer, 2001) seismic analysis software package. The b-value is a seismo-tectonic parameter directly related with the earthquake occurrence

calculated by log(N) = a - b(M) relation proposed by Gutenberg and Richter (1949), where N is the number of earthquakes with magnitude equal to or larger than M, and 'a' and 'b' are regression coefficients. The earthquake catalogue of Kandilli Observatory and Earthquake Research Institute encompassing the earthquake data between 1900 and 2016 was used (KOERI, 2016). In order to obtain a seamless and continuous b-value map, 45 km search radius was used based on the earthquake depth in the reagion reaching down to 120 km depth. Primarily, de-clustering analyses based on time and spatial windows proposed by Gardner and Knopoff (1974) was performed on the earthquake database in order to ensure that the catalogue represents Poisson relation used to represent the earthquake phenomenon in time domain, and also to ensure mutually exclusiveness of the events. Furthermore, based on the catalogue completeness principle (Stepp, 1979), events only after 1964 was used (Atakan et al., 2002, Kalkan et al., 2009). Following the exclusion of secondary events and time threshold of 1964 out of a total of 6415 events having Mw>3.0, the final de-clustered catalogue included 2350 earthquakes. The b-value map was prepared with 1 km x 1 km resolution (Figure 3f).

Another dataset is the graben center generated by utilizing 1:1250000 scale free air gravity and Bouger gravity maps (Arslan et al., 2010) as well as the geological map. This graben center data is used to generate distance to graben center map with 90 m x 90 m spatial resolution. As the well data is distributed at both sides of the graben center, the northern section is multiplied by -1 and the southern section is multiplied by +1 in order to be able to differentiate between the two flanks of the graben. The distance to graben center map is shown in Figure 3g where the Quaternary alluvium deposits are overlain on the generated map.

The final dataset is the geothermal gradient map which is the dependent variable. In order to generate this interpolation map, data from wells deeper than 200 m and having bottom hole temperatures higher than 18ºC (long term average annual temperature of the Manisa Province) were used (General Directorate of Meteorology, 2017). A total of 93 well data were included in the final dataset with bottom hole temperatures ranging between 25ºC and 260ºC and depths ranging between 250 m and 3600 m. This data was used to generate the geothermal gradient (˚C/100 m) for each location. The interpolation map was generated by using Ordinary Kriging Method which is based on assumption of normal distribution of the data. Therefore, dataset was explored and logarithmic transformation and second order trend removal were applied in order to satisfy this condition. In order to avoid extrapolation, the boundaries of the resultant map was limited to the extent of the input well dataset points and all further analyses were performed on this areal extent (Figure 3h).

Table 1: Datasets used in the analyses and their descriptive statistics.

Data Set	Source	Scale/Resolution	Descriptive Statistics for the Study Area			
			Min.	Max.	Mean	St. Dev.
Geothermal Gradient	MTA and various private sector companies	90 m x 90 m	1.95*	25*	8.14*	4.94*
Digital Elevation Model	HGK	1:25.000	5	2056	397	382
Slope		1:25.000	0	41	6.5	6.9
NDVI	Landsat 8 OLI-TIRS	30 m x 30 m	-1	+1	0.26	0.09
b-value Map	KOERİ, 2016	1 km x 1 km	1.06	1.43	1.23	0.07
Fault Density	MTA, 2002	1:500 000	0	0.66	0.19	0.16
	Yılmazel et al., 2010	1:500 000				
	Duman, et al.,2011	1:250 000				
	Klingel et al., 2015	1:700 000				
Distance to Graben Center	Arslan v.d., 2010	1:1.250.000	6	24565	7515	5104
Night-time Surface Temperature	ASTER L1T	90 m x 90 m	0	59.7	34.5	6.23
Geology	MTA, 2002	1:500 000	NA**			

* Statistics of well data is given.
** Categorical vector data.

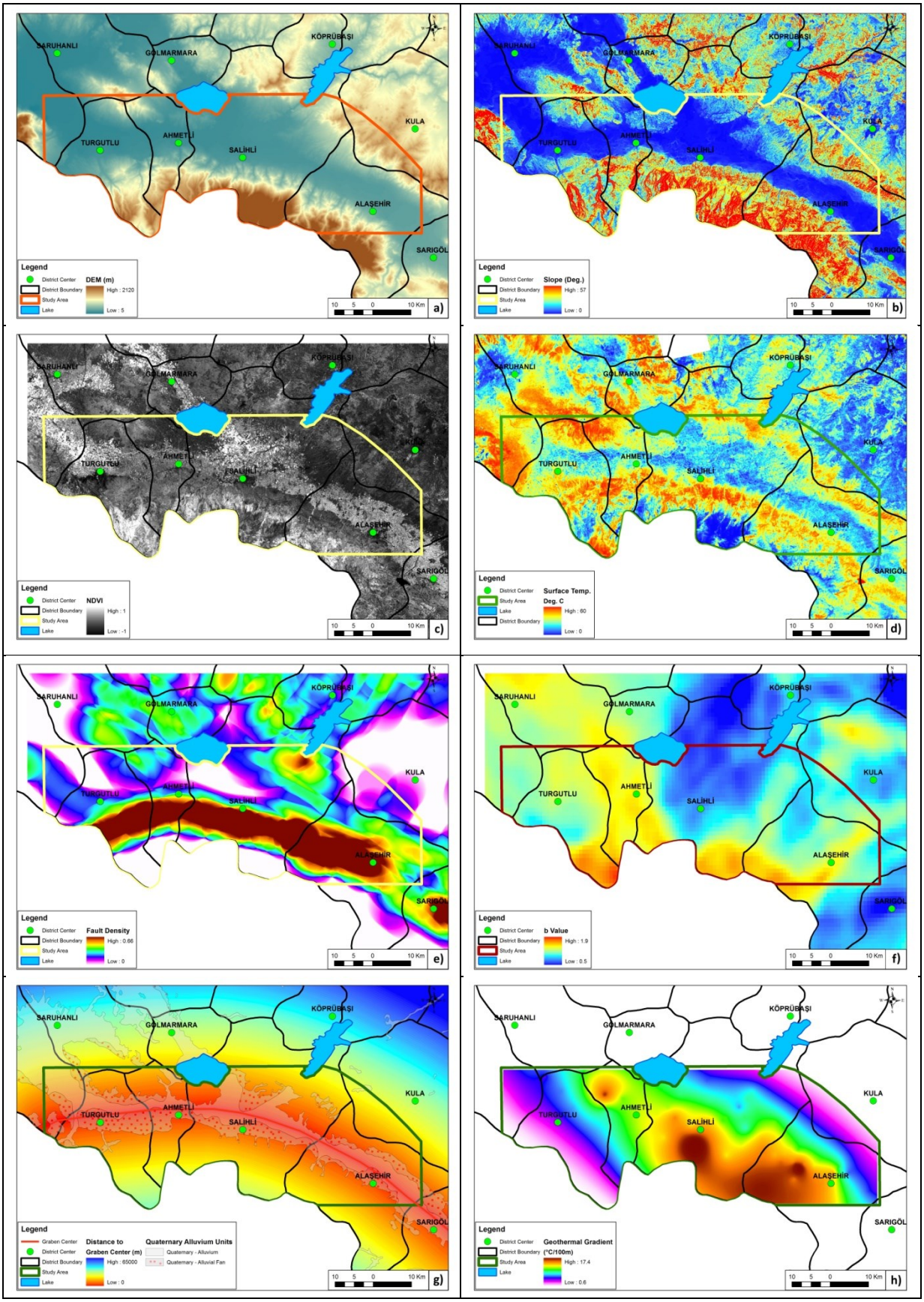

Figure 3: Collinearity statistics with geothermal gradient as dependent variable. a) Digital Elevation Model, b) Slope, c) NDVI, d) ASTER nighttime surface temperature, e) Fault density, f) b-value, g) Distance to graben center and h) Geothermal Gradient.

4. STATISTICAL ANALYSES METHODS

All variables were compiled within a GIS environment in order to ensure spatial coherence. The Pearson correlation coefficient (Pearson, 1895) was used to identify the degree of linear correlation between dependent and explanatory variables. The coefficient ranges between -1 and 1 where the sign indicates negative or positive correlation respectively and the value of the coefficient indicates the degree of correlation. Therefore, the results of a bivariate, Pearson correlation shows the degree of linear dependence between two variables.

The bivariate normal distribution assumption can be replaced with the assumption that one of the variables has normal distribution and the two variables are independent (Hogg and Craig, 1978). Therefore, each dataset was individually inspected and the necessary transformations were performed. Prior to performing bivariate correlation, multi-collinearity analysis was conducted on all variables. In the analysis, the tolerance is the percent of the variance in a given predictor that cannot be explained by the other predictors (Norusis, 2004). Low tolerance values indicate that around 70-90% variance of an explanatory variable can be explained by other explanatory variables. When the tolerance is close to 0, there exists a high multicollinearity and the standard error of the regression coefficients will be inflated. There are various suggestions for tolerance and VIF values in the literature, however, the values of 0.2 for tolerance and 5 for VIF are recommended (Menard, 1995; Rogerson, 2001).

Multicollinearity analysis was performed on the dependent variable (geothermal gradient), and the explanatory variables. The result of the multicollinearity analysis shows that no variable has a VIF value higher than 5 and thus it was concluded that no collinearity exists between the variables (Table 2). Therefore, the Pearson (bivariate) correlation analysis was performed on all variables.

Table 2: Collinearity statistics with geothermal gradient as dependent variable.

Variable	Collinearity Statistics	
	Tolerance	VIF
DEM	0.231	4.326
Slope	0.219	4.570
NDVI	0.844	1.184
b value	0.622	1.609
Fault Density	0.737	1.358
Distance to Graben Center	0.559	1.790
ASTER Nighttime Surface Temperature	0.630	1.587

5. RESULTS AND DISCUSSION

The bivariate Pearson correlation analysis was performed between the geothermal gradient and the other continuous explanatory variables; 1) DEM, 2) Slope, 3) NDVI, 4) Fault density, 5) Gutenberg-Richter b-value, 6) Distance to graben center and 7) ASTER night-time surface temperature. The geology layer is a categorical data and thus could not be included into the analysis due to assumptions of the Pearson correlation method. However, since elevation and slope data can represent distribution of Quaternary alluvium and Pliocene sedimentary data and older geological units as morphological parameters, it is considered that the lack of geology layer does not significantly affect the coherent and explanatory nature of the analyses. 72 out of 93 well data used in the analysis fall within the boundaries of the Quaternary sedimentary units including alluvium, alluvial fan and travertine deposits. 10 of the wells are located within the Plio-Quaternary carbonate deposits while 9 wells fall within the Miocene age sedimentary units and finally 2 wells fall within the Paleozoic age metamorphic units. In other words, around 88% of the entire well data falls within Quaternary and Plio-Quaternary sediment and carbonate deposits indicating that the main dataset is mostly confined in young sedimentary units which are deposited along the Gediz Graben basin area.

Table 3: Pearson correlation coefficient and P-value diagnostics of explanatory variables.

Variable	Geothermal Gradient	P (<0.05)
DEM	0.189	0.000
Slope	0.241	0.000
NDVI	0.076	0.000
b-Value	0.153	0.000
Fault Density	0.379	0.000
Distance to Graben Center	0.436	0.000
ASTER Night-time Surface Temperature	0.105	0.000

As can be seen from Table 3, all explanatory variables are statistically significant ($p < 0.05$). The Pearson coefficients of each explanatory variable against the geothermal gradient can be seen on Table 3 as well. These coefficients can be interpreted according to the correlation strength ranges, suggested by Evans (1996). According to Evans (1996), the absolute value of the Pearson coefficient can be classified as very weak (0-0.19), weak (0.20-0.39), moderate (0.40-0.59), strong (0.60-0.79) and very strong (0.80-1.0).

As can be seen from the correlation coefficients, tectonic structures, i.e., fault density and distance to graben center have the highest correlation strength having moderate positive correlation with the geothermal gradient data. This indicates that proximity to faults and structural features have the highest correlation. On the other hand the Gutenberg-Richter b-value has very weak positive correlation which may be due to the lack of events smaller than 3 in the earthquake catalogue. The NDVI values throughout the study area are almost entirely positive with a mean value of 0.22±0.09.and it shows a very weak correlation with the geothermal gradient. The ASTER night-time surface temperature data is also very weakly correlated with the geothermal gradient. This may show that even though the ASTER data is corrected for elevation, further corrections may be required in order for this dataset to be used more effectively as an explanatory variable (Coolbaugh et al., 2007; Gutierrez et al., 2012).

The morphologic parameters, DEM and slope, have weak to very weak positive correlation with the geothermal gradient data. This weak correlation could be due to fact that significant amount of the borehole data, used in the analysis, are located on an area with gentle slope. Although there is a wide range throughout the extent of the study area in terms of both elevation and slope values, the elevation values at the exact locations of the boreholes range between 32 m and 529 m with a mean value of 139 m, while the slope values range between 0 and 18º with the mean value of 2.65º. Furthermore, the distribution of the main borehole data is confined mostly to the Quaternary alluvium units and therefore a generalized Quaternary unit boundary was used to select a descriptive subset and statistical assessments were repeated (Table 4).

Table 4: Collinearity statistics and Pearson correlation results of the analysis for the Quaternary alluvium boundary.

Variable	Collinearity Statistics		Pearson Correlation Results		
	Tolerance	VIF	Geothermal Gradient	% Change from Initial Correlation	P (<0.05)
DEM	0.410	2.437	0.247	30.7	0.000
Slope	0.471	2.123	0.092	-61.8	0.000
NDVI	0.855	1.170	0.095	25.0	0.000
b value	0.853	1.172	0.114	-25.5	0.000
Fault Density	0.454	2.205	0.395	4.2	0.000
Distance to Graben Center	0.734	1.363	0.273	-37.4	0.000
ASTER Nighttime Surface Temperature	0.714	1.401	0.364	246.7	0.000

As can be observed from Table 4, when correlation coefficient values for the structural explanatory variables are investigated, fault density have remained almost the same while the correlation of distance to graben center have decreased as the graben distance variable is confined to a smaller range. As the subset is confined to a gentle topography, having mean values of 107 m and 1.4º, minor changes on the correlation coefficients accompanied with a slight increase in the correlation strength of the DEM was observed, without any overall significant improvement. The correlation strengths of NDVI and b-value variables have remained the same. The most significant change have occurred in the surface temperature explanatory variable where the correlation coefficient have increased almost by a factor of 2.5. This is probably associated with the fact that the subset is confined to a flat area with similar surface materials. This significant increase suggests that further corrections such as topographic slope, albedo and thermal inertia on surface temperature data (Coolbaugh et al., 2007; Gutierrez et al., 2012) can further improve the correlation of ASTER surface temperature data with the geothermal gradient. If the analysis were to be repeated for the entire area, after the suggested corrections, it is possible that a more significant correlation between ASTER surface temperature data and the geothermal gradient can be observed.

6. CONCLUSION

The Gediz Graben, Manisa is the second most important region in Turkey in terms of geothermal power generation with 118 MWe installed power. In this study, geothermal potential of the Gediz Graben is assessed by correlating geothermal gradient data with seven different explanatory variables encompassing the morphological factors, vegetation, seismo-tectonic parameters and surface temperature. Bottom-hole temperature and depth information from 93 wells were used to generate geothermal gradient interpolation map via Ordinary Kriging Method. Each variable was prepared with a 90 m x 90 m spatial resolution and introduced into a GIS environment bounded by the distribution of the well data. The dependent variable was compared with the seven explanatory variables (DEM, slope, NDVI, b-value, fault density, distance to graben center and ASTER nighttime surface temperature) through Pearson bivariate correlation.

The correlation results have shown that morphological and vegetation parameters which have low variance along the study area (mostly flat graben basin), have weak to very weak correlation, whereas the seismological (b-value) parameter along with ASTER nighttime surface temperature have very weak correlation with the geothermal gradient. On the other hand structural parameters fault density and distance to graben center have moderate correlation with the gradient data.

Since most of the well data is located within the Quaternary alluvium material, the analyses were repeated by subsetting the main dataset according to boundary of the alluvium deposits. Correlation results of this subset data has shown considerable increase in the correlation strength of the ASTER nighttime surface temperature variable. The correlation coefficient of the two important parameters in the initial analyses, being fault density and distance to graben center, have decreased and slightly increased, respectively. Although the correlation strengths of DEM, slope, NDVI and b-value parameters have changed, due to their weak to very weak correlation strengths, this change was not considered to be significant. One important deduction upon comparison of these two statistical analyses is that the performance of the ASTER surface temperature data can be improved via performing further corrections on the image data in order to eliminate the effects of material (albedo), topography and thermal inertia.

It can be concluded that the analyses results may be further improved if a denser well data distribution, an earthquake catalogue including smaller magnitudes, and ASTER images with further corrections are employed. However, current results suggest that the structural identifiers being fault density and distance to graben center data are the most descriptive variables.

REFERENCES

Arslan, S., Akın, U., and Alaca, A.: Assessment of Crustal Structure of Turkey with Gravity Data, *MTA Dergisi*, 140, (In Turkish) (2010), 57-73.

Atakan, K., Ojeda, A., Meghraoui, M., Barka, A., Erdik, M., and Bodare, A.: Seismic Hazard in Istanbul Following the 17 August 1999 Izmit and 12 November 1999 Duzce Earthquakes, *Bull. Seismol. Soc. Am.,* 92 (1), (2002), 466-482.

Boullier, A.M., Charoy, B., Pollard, P.J.: Fluctuation In Porosity And Fluid Pressure During Hydrothermal Events: Textural Evidence in The Emuford District, *Australia. J. Struct. Geol*., 16 (10), (1994), 1417–1429.

Calvin, W.M., Coolbaugh, M., Kratt, C., Vaughan, R. G., and Calvin, W.: Application of Remote Sensing Technology to Geothermal Exploration, *Geological Survey of Nevada*, (2005).

Carranza E.J.M., Wibowo, H., Barritt, S.D., and Sumintadireja, P.: Spatial Data Analysis and Integration for Regional-Scale Geothermal Potential Mapping, West Java, Indonesia, *Geothermics,* 37, (2008), 267-299.

Coolbaugh, M. F., Taranik, J. V., Rains, G. L., Shevenell, L. A., Sawatzky, D. L., Bedell, R., and Minor, T. B.: A Geothermal GIS for Nevada: Defining Regional Controls and Favorable Exploration Terrains for Extensional Geothermal Systems, *Transactions-Geothermal Resources Council*, (2002), 485-490.

Coolbaugh, M. F., and Shevenell, L. A.: A Method for Estimating Undiscovered Geothermal Resources in Nevada and the Great Basin, *Geothermal Resources Council Transactions*, 28, (2004), 13-18.

Coolbaugh, M. F., Kratt, C., Fallacaro, A., Calvin, W. M., and Taranik, J. V.: Detection of Geothermal Anomalies Using Advanced Spaceborne Thermal Emission and Reflection Radiometer (ASTER) Thermal Infrared Images at Bradys Hot Springs, Nevada, USA, *Remote Sensing of Environment*, 106 (3), (2007), 350-359.

Curewitz, D., and Karson, J.A.: Structural settings of hydrothermal outflow: Fracture Permeability Maintained by Fault Propagation and Interaction, *Journal of Volcanology and Geothermal Research,* 79, (1997), 149-168.

Duman, T.Y., Emre, Ö., Doğan, A., Özalp, T., and Elmacı, H.: 1:250.000 Scale Active Fault Maps of Turkey, *Maden Tetkik Arama (MTA),* Ankara-Turkey, (2011).

Elders, W.A., Bird, D.K., Williams, A.E., and Schiffman, P.: Hydrothermal Flow Regime and Magmatic Heat Source of the Cerro Prieto Geothermal System, Baja California, Mexico, *Geothermics,* 13, (1984), 27 - 47.

Embley, R.W., Chadwick, W.W., Jonasson, I.R., Butterfield, D.A., and Baker, E.T.: Initial Results of the Rapid Response to the 1993 Coaxial Event: Relationships Between Hydrothermal And Volcanic Processes, *Geophys. Res. Lett*., 22 (2), (1995), 143–146.

Eneva, M., Coolbaugh, M., Bjornstad, S., and Combs, J.: Detection Of Surface Temperature Anomalies in the Coso Geothermal Field Using Thermal Infrared Remote Sensing, *Geothermal Resources Council Transactions*, 31, (2007), 335-340.

Eneva, M., Coolbaugh, and M. Combs, J.: Application of Satellite Thermal Infrared Imagery to Geothermal Exploration in East Central California, *Geothermal Resources Council Transactions*, 30, (2006), 407-411.

Evans, J.D.: Straightforward Statistics for the Behavioral Sciences, Pacific Grove, CA, *Brooks/Cole*, (1996).

Faulds, J.E., Hinz, N.H., Coolbaugh, M.F., Cashman, P.H., Kratt, C., Dering, G., Edwards, J., Mayhew, B., and McLachlan, H.: Assessment of Favorable Structural Settings of Geothermal Systems in the Great Basin, Western USA, *Geothermal Resources Council Transactions,* 35, (2011), 777-783.

Gardner, J.K. and Knopoff, L.: Is the Sequence of Earthquakes in Southern California, with Aftershocks Removed, Poissonian?, *Bulletin of the Seismological Society of America*, 64, (1974), 1363-1367.

Gillespie, A., Rokugawa, S., Matsunaga, T., Cothern, J. S., Hook, S., and Kahle, A. B.: A Temperature And Emissivity Separation Algorithm for Advanced Spaceborne Thermal Emission and Reflection Radiometer (ASTER) Images, *IEEE Transactions on Geoscience and Remote Sensing,* 36, (1998), 1113−1126.

Gutenberg, B., and Richter, C.F.: Seismicity of the Earth and Associated Phenomenon, Princeton University Press, *Princeton, New York*, (1949).

Gutiérrez, F.J., Lemus, M., Parada, M.A., Benavente, O.M. and Aguilera, F.A.: Contribution of ground surface altitude difference to thermal anomaly detection using satellite images: Application to volcanic/geothermal complexes in the Andes of Central Chile. Journal of Volcanology and Geothermal Research, (2012), 237, pp.69-80.

Haselwimmer, C., Prakash, A.: Thermal Infrared Remote Sensing of Geothermal Systems. In Thermal Infrared Remote Sensing, (2013) 453-473.

Henley, R.W., Brown, K.L.: A practical guide to the thermodynamics of geothermal fluids and hydrothermal ore deposits. In: Berger, B.R., Bethke, P.M. (Eds.), Geology and Geochemistry of Epithermal Systems. Rev. Econ. Geol. (1985) 2, 25 - 43.

Hogg, R.V., Craig, A.T., 1978. Introduction to Mathematical Statistics, Macmillan Publishing Co., Inc., Newyork.

Hook, S. J., Gabell, A. R., Green, A. A. and Kealy, P. S.: A comparison of techniques for extracting emissivity information from thermal infrared data for geologic studies. Remote Sensing of Environment, (1992) Vol. 42, pp. 123-135.

Kalkan, E., Gulkan, P., Yilmaz, N., and Celebi, M., 2009, Reassessment of Probabilistic Seismic Hazard in the Marmara Region, Bull. Seismol. Soc. Am., 99 (4), 2127-2146.

Klingel, E., Tavlan, M., Ozcetin, K. and de Wijkerslooth, C., Geothermal Exploration Where Innovative Meets Classic Geothermal Exploration in Western Anatolia, *Proceedings World Geothermal Congress 2015 Melbourne, Australia*, (2015)

KOERI: Earthquake Catalogue (http://www.koeri.boun.edu.tr/sismo/2/earthquake-catalog/, access date: December,30 .2016, (2016).

Lachenbruch, A.H.: Frictional Heating, Fluid Pressure, and the Resistance to Fault Motion, *J. Geophys. Res*. 85, (1980), 6097-6112.

MacKnight IV, R.B., Silver, E., Kennedy-Bowdoin, T., Pickles, W.L., and Waibel, A.: Remote Sensing Analysis of Structure and Geothermal Potential of the Humboldt Block, Nevada, *Geoscience and Remote Sensing Symposium*, *IEEE International 1*, (2004).

Marques, J.M., Matias, M.J., Basto, M.J., Carreira, P.M., Aires-Barros, L.A., and Goff, F.E.: Hydrothermal Alteration of Hercynian Granites, Its Significance to the Evolution of Geothermal Systems in Granitic Rocks, *Geothermics,* 39, (2010), 152-160.

Martel, S.J., and Petersen, J.E.: Interdisciplinary Characterization of Fracture Systems at the US/BK Site, Grimsel Laboratory, Switzerland, *Int. J. Rock Mech. Min. Sci., Geomech. Abstr*., 28(4), (1991), 295–323.

McKenzie, D.: Some remarks on the development of sedimentary basins, *Earth Planet. Sci. Lett*., 40, (1978), 25–32.

Menard, S.: Applied Logistic Regression Analysis: Sage University Series on Quantitative Applications in the Social Sciences, *Thousand* Oaks*, CA: Sage.,* (1995).

Micklethwaite, S., and Cox, S.F.: Fault-Segment Rupture, After Shock Zone Fluid Flow, and Mineralization, *Geology,* 32(9), (2004), 813-816.

MTA: 1/500.000 Scale Geological Maps, (2002).

NASA LP DAAC.: Aster Level 1 Precision Terrain Corrected Registered At-Sensor Radiance V003, Nasa Eosdis Land Processes Daac. Doi:10.5067/Aster/Ast_L1t.003, (Http://Earthexplorer.Usgs.Gov/) Accessed On January 15, 2017, (2015).

Noorollahi, Y., Itoi, R., Fujii, H., and Tanaka, T.: GIS Integration Model for Geothermal Exploration and Well Siting, *Geothermics*, (2008), 37, 107-131.

Norusis: SPSS 13.0 guide to data analysis. Upper Saddle-River, NJ, *Prentice Hall*, Inc. (2004).

Özgüler, M.E., Turgay, C., and Şahin, H.: Geophysical studies in Denizli geothermal field, *MTA J. 99–100:129–142* (in Turkish), (1983).

Pearson, K.: Notes on Regression and Inheritance in the Case of Two Parents, *Proceedings of the Royal Society of London*, 58, (1895), 240–242

Person, M., Raffensperger, J.P., Ge, S., and Garvin, G.: Basin-scale Hydrogeologic Modeling, *Rev. Geophys*., 34(1), (1996), 61–87.

Prol-Ledesma R.M.: Evaluation of the Reconnaissance Results in Geothermal Exploration Using GIS, *Geothermics,* 29, (2000), 83–103.

Rogerson, P. A.: Statistical Methods for Geography, *London: Sage*, (2001).

Scholz, C.H.: Shear Heating and the State of Stress on Faults, *J. Geophys. Res*., 85, (1980), 6174 - 6184.

Shah, S.T.: Stress Tensor Inversion From Focal Mechanism Solutions and Earthquake Probability Analysis of Western Anatolia, Turkey, *Doctoral Dissertation, Middle East Technical University*, (2015).

Stepp, J.C.: Analysis of Completeness of the Earthquake Sample in the Puget Sound Area, *In Contributions to seismic zoning: U.S. National Oceanic and Atmospheric Administration Technical Report ERL 267-ESL* 30 *(edited by Harding, S. T.),* (1973), 16-28.

Tüfekçi, N., Süzen, M.L., Güleç, N.: GIS Based Geothermal Potential Assessment: A Case Study from Western Anatolia, Turkey, *Energy*, 35, (2010), 246-261.

Voulgaris, N., Parcharidis, I., Pahoula, M., and Pirlis, E.: Correlation of Tectonic, Seismicity and Geothermics of Lesbos Island Using Remote Sensing Data and Geographical Information System, *Bulletin of the Geological Society of Greece*, 36, 2004, 938-947.

Wohletz, K., and Heiken, G.: Volcanology and Geothermal Energy, *Univ. California Press, Berkeley and Los Angeles, CA,* (1992), 432p.

Yilmaz, Y., Genç, Ş.C., Gürer, F., Bozcu, M., Yilmaz, K., Karacik, Z., Altunkaynak, Ş. and Elmas, A.: When did the western Anatolian grabens begin to develop?. Geological Society, London, Special Publications, (2000), 173(1), pp.353-384.

Yilmazer, S., S. Pasvanoglu, and S. Vural.: The relation of geothermal resources with young tectonics in the Gediz graben (West Anatolia, Turkey) and their hydrogeochemical analyses, *In Proceedings World Geothermal Congress*, (2010), pp. 1-10.

Yousefi, H., Ehara, S., and Noorollahi, Y. :Geothermal Potential Site Selection Using GIS in Iran, *Proceedings*, Thirty-Second Workshop on Geothermal Reservoir Engineering Stanford University, Stanford, California, SGP-TR-183, (2007).